

Shark skin effect in creeping films

M. Scholle and N. Aksel*

*Department of Applied Mechanics and Fluid Dynamics,
University of Bayreuth, Universitätsstraße 30, D-95440 Bayreuth, Germany*

(Dated: June 16, 2018)

If a body in a stream is provided with small ridges aligned in the local flow direction, a remarkable drag reduction can be reached under turbulent flow conditions. This surprising phenomenon is called the 'shark skin effect'. We demonstrate, that a reduction of resistance can also be reached in creeping flows if the ridges are aligned perpendicular to the flow direction. We especially consider in gravity-driven film flows the effect of the bottom topography on the mean transport velocity.

PACS numbers: 47.15.Gf

INTRODUCTION

It is yet controversially discussed that the dermal surface morphology of sharks is in order to improve the sharks' swimming performance [1]. Nevertheless, it is widely accepted that for bodies in turbulent flows a reduction of skin friction by some percent can be reached if the surface of the body is provided with small ridges aligned in the local flow direction [2, 3]. This rather counter-intuitional phenomenon occurs in turbulent flows if the riblet spacing is smaller than the typical diameter of the streamwise vortices such that the vortices are forced to stay above the riblets and touch only the tips of the riblets.

The criterion for turbulent flow conditions is based on the Reynolds number

$$\text{Re} := \frac{\rho UL}{\eta}, \quad (1)$$

which gives a comparison between inertial forces and friction forces. By U and L a characteristic flow velocity and a characteristic length of the system are denoted, ρ and η are the mass density and the dynamic viscosity of the fluid. At high Reynolds numbers, typically 10^4 or larger, the flow is turbulent and vortices are created due to inertia. At small Reynolds number the flow is laminar and at vanishingly small Reynolds numbers $\text{Re} \ll 1$ the flow is creeping. Hence, in creeping flows a 'shark skin effect' is not expected since inertia-induced vortices are absent.

If the the riblets are aligned perpendicular to the flow direction, however, kinematically induced vortices can be created even in creeping flows where inertia is absent [4, 5]. We especially consider a steady, gravity-driven film flow of an incompressible Newtonian fluid on an inclined plane. The bottom of the inclined plane is provided with periodic corrugations according to FIG. 1. The mean film thickness is denoted by H , the periodic length by λ and the mean inclination angle by α . A Cartesian coordinate system is used with the x -axis placed at the mean level of the bottom contour, the y -axis in line with the ridges and the z -axis normal to the mean level of the bottom.

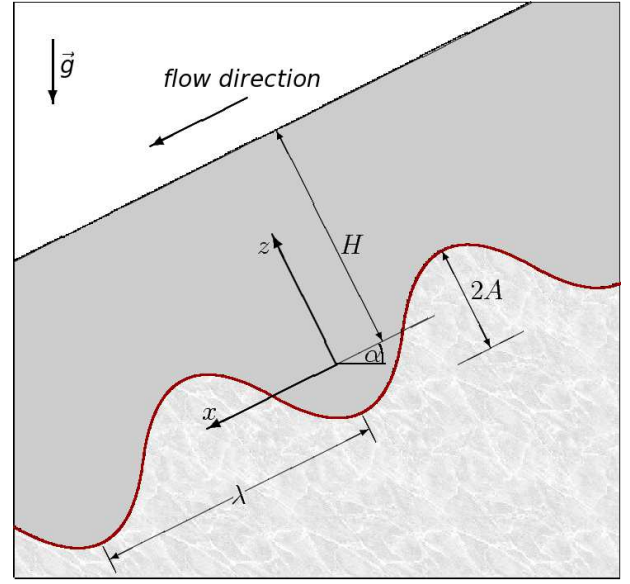


FIG. 1: Sketch of the flow geometry

MATHEMATICAL FORMULATION

Basic equations and solving procedure

The basic field equations are the continuity equation and the Navier–Stokes equations [6]

$$\nabla \cdot \vec{v} = 0, \quad (2)$$

$$\rho \left[\frac{\partial \vec{v}}{\partial t} + (\vec{v} \cdot \nabla) \vec{v} \right] = -\nabla p + \eta \nabla^2 \vec{v} + \rho \vec{g}. \quad (3)$$

By \vec{g} the gravity acceleration is denoted. The bottom contour is in general characterised by a 2π -periodic function $b(\hat{x})$ as $z = b(2\pi x/\lambda)$. Along the bottom the flow fulfills the no-slip condition

$$\vec{v} = \vec{0}. \quad (4)$$

Assuming that the film height exceeds the wavelength of the bottom, the curvature of the free surface can be neglected [5, 7]. Then, the free surface is given as $z = H$.

At the free surface the dynamic boundary condition

$$\vec{e}_z \{ [\tilde{p} - \tilde{p}_s] \underline{\underline{1}} - \eta [\nabla \otimes \vec{v} + (\nabla \otimes \vec{v})^T] \} = \vec{0}, \quad (5)$$

which is the equilibrium between pressure jump at the surface and viscous forces, has to be fulfilled. By p_s the pressure of the surrounding is denoted. If the spatial extensions of the bottom in y -direction are sufficiently large, side wall effects can be neglected and a two-dimensional flow geometry can be assumed. This allows for a representation of the velocity field in terms of a stream function, i.e.

$$\vec{v} = \frac{\partial \psi}{\partial z} \vec{e}_x - \frac{\partial \psi}{\partial x} \vec{e}_z \quad (6)$$

by which the continuity equation (2) is identically fulfilled. Since due to the creeping condition $\text{Re} \ll 1$ the inertia terms at left hand of the Navier–Stokes equations are negligible, EQ. (3) simplifies to the Stokes equations

$$\vec{0} = -\nabla p + \eta \nabla^2 \vec{v} + \varrho \vec{g}. \quad (7)$$

Reconsidering EQ. (6), the solution of Stokes equations is explicitly given as [5]

$$\psi = \frac{\varrho g H^3 \sin \alpha}{2\eta} \left[\frac{z^2}{H^2} - \frac{z^3}{3H^3} + \Re \left[r(\xi) + \frac{z}{H} q(\xi) \right] \right], \quad (8)$$

$$p = p_s + \varrho g \left[(H - z) \cos \alpha + \frac{\pi H^2 \sin \alpha}{\lambda} \Im q'(\xi) \right], \quad (9)$$

where $q(\xi)$ and $r(\xi)$ are holomorphic functions of the complex variable

$$\xi := \pi \frac{z + ix}{\lambda}. \quad (10)$$

The symbols \Re and \Im denote the real and imaginary part of a complex expression, the prime derivation with respect to ξ . By inserting the general solution (8, 9) in the boundary conditions (4, 5), a set of equations for the boundary values of the two holomorphic functions $q(\xi)$ and $r(\xi)$ is derived. Due to the periodicity of the flow a representation of the boundary values of $q(\xi)$ and $r(\xi)$ by Fourier series can be applied, which leads to an algebraic set of equations for the series coefficients. After truncating to a finite number of Fourier modes, its solution is determined by using computer algebra, e.g. MAPLE. The above method and the solving procedure is described in detail in [5]. For the calculations presented here the series have been truncated at the mode number where the values of the coefficients fall below 10^{-10} . This leads to truncation orders between 12 and 36.

Bottom shapes

For the modelling of wall roughness Panton [8] suggests a 'brush model', i.e. an infinite array of equidistant

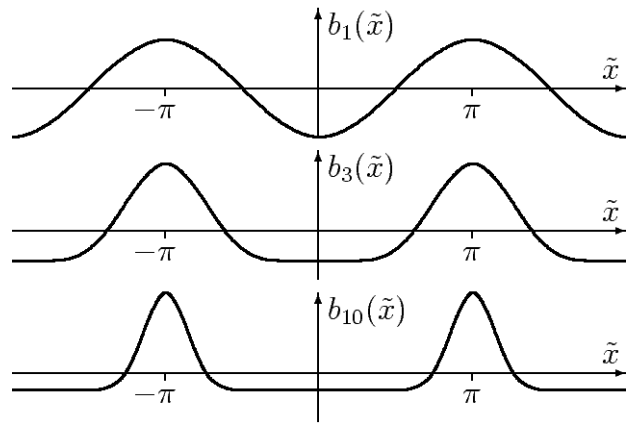


FIG. 2: The three different bottom shapes b_1 , b_3 and b_{10} .

narrow peaks. We approach this strongly idealised shape by three different trigonometric polynomials as shown in FIG. 2. At first, we consider a harmonic contour, i.e.

$$b_1(\tilde{x}) = -A \cos \tilde{x}, \quad (11)$$

with amplitude A as a comparatively smooth shape. In contrast to this, by the third order trigonometric polynomial

$$b_3(\tilde{x}) = -\frac{A}{16} [15 \cos \tilde{x} - 6 \cos 2\tilde{x} + \cos 3\tilde{x}] \quad (12)$$

an array of peaks is given. Since the derivatives of $b_3(\tilde{x})$ up to the 5th order vanish, a flat region between the peaks becomes apparent. The parameter A is again the amplitude, in the sense that $b_3(\pi) - b_3(0) = 2A$. The third shape shown in FIG. 2, which is defined as

$$b_{10}(\tilde{x}) = -\frac{A}{262144} [167960 \cos \tilde{x} - 125970 \cos 2\tilde{x} + 77520 \cos 3\tilde{x} - 38760 \cos 4\tilde{x} + 15504 \cos 5\tilde{x} - 4845 \cos 6\tilde{x} + 1140 \cos 7\tilde{x} - 190 \cos 8\tilde{x} + 20 \cos 9\tilde{x} - \cos 10\tilde{x}], \quad (13)$$

is an array of significantly narrower peaks than in the case $b_3(\tilde{x})$. Note, that the derivatives of $b_{10}(\tilde{x})$ vanish up to the 19th derivative. Therefore, $b_{10}(\tilde{x})$ is a good approximation for the idealised array of brush-like peaks by a continuous bottom shape.

RESULTS

Streamlines and vortex creation

Streamline patterns have been calculated for various shapes, amplitudes and film heights. For small amplitudes the streamlines follow the bottom contour, whereas flow separation is observed if the amplitude exceeds a critical limit. As representative examples in FIG. 3 the

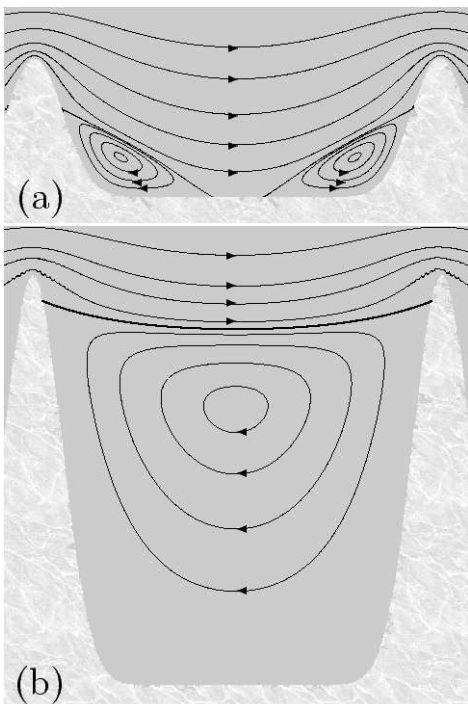


FIG. 3: Near-bottom streamlines of film flows over the shape b_{10} with amplitude (a) $A = 0.17\lambda$ and (b) $A = 0.5\lambda$.

streamlines in the vicinity of the bottom are presented for the shape b_{10} with two different amplitudes, namely $A = 0.17\lambda$ and $A = 0.5\lambda$. The film heights, $H = 1.70\lambda$ in (a) and $H = 2.24\lambda$ in (b), are chosen in order to receive the same flow rate in both cases.

The critical amplitude for the primary flow separation is $A \approx 0.107\lambda$. Thus, in FIG. 3a flow separation is already apparent: A vortex pair has been created at the positions of maximum curvature. With increasing amplitude the vortices are growing, which leads to the merging of the two vortices to a single one. Such a case with a large single vortex which covers the major part of the region between two neighbouring peaks is shown in FIG. 3b. In this example we especially see a slightly curved separatrix passing nearly from tip to tip. This feeds the hope of a probable resistance reduction, since the vortices are supposed to act like 'fluid roller bearings'. By increasing the amplitude further, a secondary vortex pair is created at the critical amplitude $A \approx 0.606\lambda$ for secondary flow separation.

Mean transport velocity

We define the mean transport velocity as

$$u_t := \frac{\dot{V}}{H_t}, \quad (14)$$

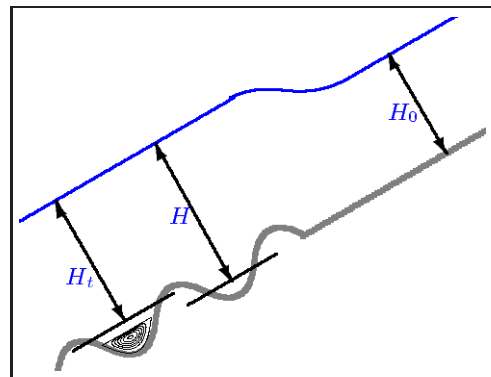


FIG. 4: The quantities H_t , H and H_0 .

where the two-dimensional flow rate is given as

$$\dot{V} = \int_{b(2\pi x/\lambda)}^H u dz = \psi(x, H) - \psi(x, b(2\pi x/\lambda)). \quad (15)$$

The quantity H_t , subsequently called the mean transport thickness, has to be understood as mean thickness of the part of the flow which contributes to the material transport, i.e. the film above the separation areas. If the separatrix of the primary vortex is given as $z = s(x)$, $x_1 \leq x \leq x_2$, the mean transport thickness results in

$$H_t := H - \frac{1}{\lambda} \int_{x_1}^{x_2} [s(x) - b(2\pi x/\lambda)] dx. \quad (16)$$

The quantity H_t has to be carefully distinguished from the mean geometrical film thickness H of the entire film which includes the vortices. Furthermore, by

$$H_0 := \left(\frac{3\eta\dot{V}}{\rho g \sin \alpha} \right)^{\frac{1}{3}} \quad (17)$$

the reference thickness of a film flow on a plane bottom with the same flow rate as the flow over the topography is defined [5]. The three quantities H_0 , H and H_t are illustrated in FIG. 4. Thus, for a fixed flow rate \dot{V} , the comparison of the mean transport thickness H_t with the reference thickness H_0 delivers an adequate measure for enhancement or reduction of the mean transport velocity in the film: In case of $H_t > H_0$, the mean transport velocity is reduced, whereas $H_t < H_0$ indicates enhancement of u_t .

In FIG. 5 the relative film elevation $(H_t - H_0)/H_0$ is plotted versus the amplitude A for the three different bottom contours b_1 , b_3 and b_{10} . This parameter study has been carried out with a fixed flow rate of $\dot{V} = 9\rho g \lambda^3 \sin \alpha / (8\eta)$, corresponding to a reference thickness of $H_0 = 3\lambda/2$. Additionally, the onset of primary and further flow separation is indicated in the diagram.

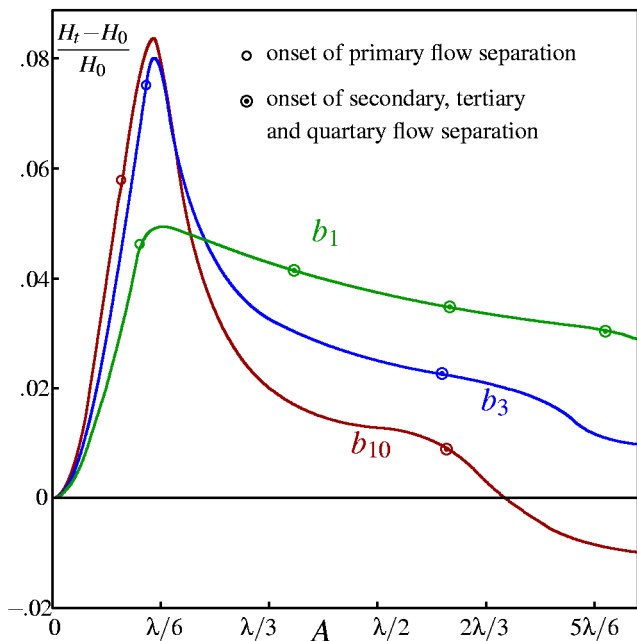


FIG. 5: Relative film elevation vs. amplitude of flows over different shapes.

From the beginning up to an amplitude of about $\lambda/6$, the film elevation is monotonously increasing for all three different shapes, which indicates a reduction of the mean transport velocity due to the bottom corrugations. Note, that within this parameter regime no positive effect can be expected since no vortices are present. However, the curves reach maxima slightly after the primary vortex generation and pass then into a monotonous decrease due to reduction of friction by vortices, which act like fluid roller bearings. Obviously, both the height of the maximum as well as the decrease after the vortex generation are more pronounced for bottom shapes with sharper peaks. For the curve associated to the bottom b_{10} the film elevation becomes negative for high amplitudes, i.e. the mean transport velocity exceeds the corresponding mean transport velocity of the flow over a plane bottom. At the highest amplitude considered in our calculations, $A = 0.9\lambda$, this enhancement of the mean transport velocity reaches 0.88%.

The increase of the mean transport velocity indicates an improved mass transport in the volume. In contrast to this, the surface velocity remains nearly unchanged.

CONCLUSION

The parameter studies on the three different shapes b_1 , b_3 and b_{10} revealed a noticeable effect of the bot-

tom topography on the material transport in a creeping film flow: For the shapes b_1 and b_3 we found a decrease of the mean transport velocity compared to the flow over a plane bottom, whereas for the shape b_{10} with the sharpest peaks an increase of the mean transport velocity becomes apparent at sufficiently high amplitude. Thus, a comparison to the 'shark skin effect', which has been successfully applied to ships and airplanes for drag reduction, is near at hand. The present effect, however, is essentially different from the popular shark skin effect: The increase of the mean transport velocity has been calculated for creeping flows, whereas the shark skin effect occurs in turbulent flow at Reynolds numbers $\approx 10^4$ – 10^6 . Furthermore, the rippled structures of the shark skin are directed longitudinal to the flow, not transversal as it is the case here. Finally, the responsible mechanism for the shark skin effect is according to [9] and [3] the control of the streamwise vortices in the turbulent flow, which has been created by inertia. In contrast to this, the rippled bottom structure in creeping film flows enforce the creation of vortices which act on the flow like a kind of 'fluid roller bearing'. Nevertheless, a common feature of the shark skin effect and the effect observed in the present paper is the reduction of resistance in the flow by means of rippled wall structures.

The highest relative increase of the mean transport velocity is in our calculations 0.88%. This is less than the shark skin effect in turbulent flow, which is supposed to be at most 10% [3]. It is an open question up to which extend the value of 0.88% can be improved by varying the relevant parameters, especially the bottom shape.

* tms@uni-bayreuth.de

- [1] S. Vogel, *Life in Moving Fluids* (Princeton University Press, 1996).
- [2] H. W. Liepmann, ed., *On the possibility of drag reduction with the help of longitudinal ridges in the walls* (Springer, 1988).
- [3] K. Koeltzsch, A. Dinkelacker, and R. A. Grundmann, *Exp. Fluids* **33**, 346 (2002).
- [4] C. Pozrikidis, *J. Fluid Mech.* **188**, 275 (1988).
- [5] M. Scholle, A. Wierschem, and N. Aksel, *Acta Mech.* **168**, 167 (2004).
- [6] J. H. Spurk, *Fluid Mechanics* (Springer, 1997).
- [7] A. Wierschem, M. Scholle, and N. Aksel, *Phys. Fluids* **15**, 426 (2003).
- [8] R. L. Panton, *Incompressible Flow* (Wiley Interscience, 1996).
- [9] W. Nachtigall, *Bionik — Grundlagen und Beispiele für Ingenieure und Naturwissenschaftler* (Springer, 2002).